

Quantum oscillations and subband properties of the two-dimensional electron gas at the $\text{LaAlO}_3/\text{SrTiO}_3$ interface

A McCollam¹, S Wenderich², M K Kruize², V K Guduru¹, H J A Molegraaf², M Huijben², G Koster², D H A Blank², G Rijnders², A Brinkman², H Hilgenkamp², U Zeitler¹ and J C Maan¹

¹High Field Magnet Laboratory, Institute for Molecules and Materials, Radboud University Nijmegen, 6525 ED Nijmegen, The Netherlands.

²Faculty of Science and Technology and MESA+ Institute for Nanotechnology, University of Twente, 7500 AE Enschede, The Netherlands.

E-mail: A.McCollam@science.ru.nl

Abstract. We have performed high field magnetotransport measurements to investigate the interface electron gas in $\text{LaAlO}_3/\text{SrTiO}_3$ heterostructures. Shubnikov-de Haas oscillations reveal several 2D conduction subbands with carrier effective masses between 1 and 3 m_e , quantum mobilities of order 3000 $\text{cm}^2/\text{V s}$, and band edges only a few millielectronvolts below the Fermi energy. Measurements in tilted magnetic fields confirm the 2D character of the electron gas, and show evidence of inter-subband scattering.

1. Introduction

It is now well-established that a two-dimensional electron gas (2DEG) can exist at the interface between perovskite oxides LaAlO_3 (LAO) and SrTiO_3 (STO) [1, 2]. The 2DEG is nominally similar to those in semiconductor heterostructures, but supports additional phases, such as superconductivity and magnetism, which are not observed in conventional 2D electron systems, and which have great fundamental and technological interest [3, 4]. The mechanism of formation of this oxide 2DEG, however, is not established, and although there is a general consensus that the charge carriers occupy STO conduction bands modified by the presence of the interface [2, 5], the origin and density of the 2D carriers, and the details of the electronic bandstructure at the interface are not yet fully understood.

Three main scenarios have emerged as the possible source of conduction electrons: ‘electronic reconstruction’, where a build-up of electric potential across the polar LAO layers is avoided by charge transfer from LAO to STO [6, 2]; donation of electrons by oxygen vacancies in the heterostructure [7, 8, 9]; and cationic intermixing and disorder across the interface [10, 11]. The relative contributions of these mechanisms seem to be determined by factors such as the sample growth conditions, the LAO layer thickness, and the overall integrity of the crystal structure. Electronic reconstruction is widely proposed to be the dominant mechanism in *intrinsic* samples, where defects, impurities and disorder are minimised, but experiments have identified a number of inconsistencies in this simple picture [5, 12, 13, 14, 15, 16], and the origin of the conduction electrons and the nature of their confinement at the interface are still unresolved questions.

Quantum oscillations in the transport (or thermodynamic) properties of metallic and semiconducting materials arise directly from the magnetic field dependence of the conduction electron energies, and are, therefore, a powerful experimental probe of the electronic bandstructure close to the Fermi energy [17]. They also provide band-specific details of conduction electron properties such as effective mass and mobility. Access to this information in LAO/STO is highly desirable, as the bandstructure of the 2DEG can be expected to reflect the mechanism of its formation, as well as giving further insight into its behaviour.

Previous quantum oscillation experiments on LAO/STO [9, 18, 19] measured the Shubnikov-de Haas (SdH) effect in the resistivity, and could clearly resolve only a single oscillation frequency corresponding to a single conduction band with high mobility charge carriers. In samples with high carrier density (of order 10^{16} cm^{-2}) [9] the oscillations were independent of the magnetic field direction, and indicated a three-dimensional Fermi surface containing all of the charge carriers. These samples were grown under conditions of low oxygen partial pressure ($< 10^{-5} \text{ mbar}$), and the high carrier density and mobility were believed to arise from uniform doping of the STO substrate by oxygen vacancies. In references 19 and 20, measurements were carried out on samples grown or annealed under higher oxygen pressures, with carrier densities of the order of 10^{13} cm^{-2} , thought to be characteristic of intrinsic samples with few or no

oxygen vacancies. These groups report slightly different values for the SdH frequency but, in both cases, the observed conduction band is two-dimensional, with very low carrier density compared to the total carrier density extracted from the Hall effect (of order 20%). These results raised interesting questions about the presence of conduction channels which do not contribute to the SdH effect, or the possibility of multiple valley and spin degeneracies [18, 19], and suggested that the LAO/STO conduction-bandstructure is considerably more complex than implied by the single observed SdH frequency. A complex bandstructure is also predicted by density-functional calculations, which give a large number of subbands, with quite different carrier properties, crossing the Fermi energy [20, 21, 22].

In this work, we present a detailed magnetotransport investigation of LAO/STO-based heterostructures, as a function of temperature and in a range of magnetic field orientations, from perpendicular to parallel to the oxide layers. By using very high magnetic fields and high-mobility 2DEGs, we have been able to measure Shubnikov-de Haas oscillations with significantly better resolution than previously possible, and have identified and characterised several 2D conduction subbands. The subbands are separated by a few millielectronvolts, and have different effective masses and mobilities. We find a total carrier density of $\sim 10^{13} \text{ cm}^{-2}$ contributing to the SdH effect.

2. Experiments and results

We have measured three heterostructures (labelled S1, S2 and S3), with the same basic structure, but differing slightly in the number of LAO layers or in the oxygen partial pressure during growth. The samples were grown by pulsed laser deposition, with ten (S1, S3) or nine (S2) monolayers of LAO deposited on a TiO_2 -terminated STO(001) substrate. A single monolayer of SrCuO_2 (SCO) and two monolayers of STO were grown as capping layers on top of the LAO, as illustrated in Fig. 1(d). Oxygen partial pressure of 2×10^{-3} mbar was used during LAO growth for S1 and S2, and this was reduced to 1×10^{-5} mbar for S3. Full details of the growth procedure and parameters are given as Supplementary Information.

The role of the SCO layer is, at present, not fully understood, but we find that it considerably increases the mobility of the LAO/STO interface (compared to samples prepared in an identical way, but without SCO) [23]. We find no evidence of a conducting channel at isolated SCO/LAO or SCO/STO interfaces, and assume that the single monolayer of SCO in our heterostructures does not contribute directly to the conductivity by supporting an additional 2DEG. Rather, the SCO layer is thought to indirectly enhance the mean free path of mobile electrons at the LAO/STO interface by somehow reducing the density of defect donor states in the structure. A detailed investigation of the effect of the SCO layer is presented elsewhere [23].

Our samples had dimensions of $5 \text{ mm} \times 5 \text{ mm}$ in the xy plane, with electrical contacts made by wire bonding through the top surface in a van der Pauw geometry. Resistance was measured using a standard ac technique with excitation currents of 1 or

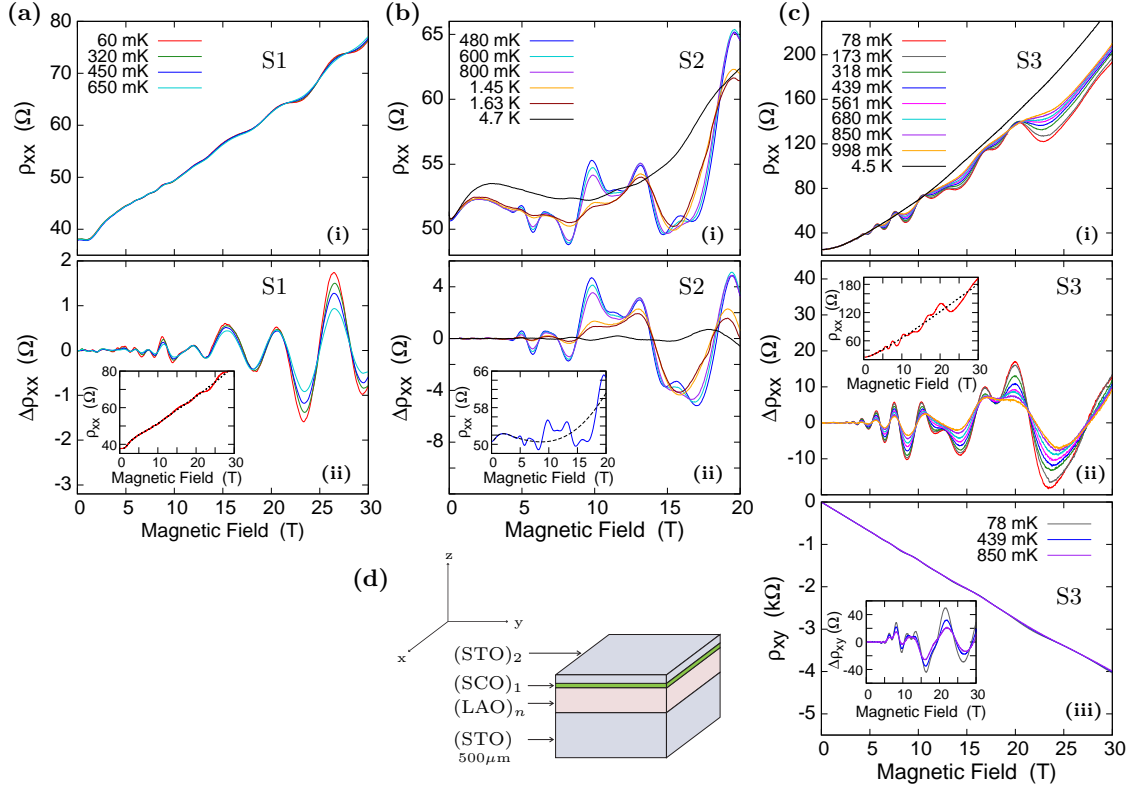


Figure 1. (a)–(c)(i): Temperature dependence of ρ_{xx} in samples S1, S2 and S3. (a)–(c)(ii): The oscillations in (i) with background removed. An example of the background subtracted in each case is shown as a dashed line in the insets. (c)(iii): Hall effect of sample S3. The inset shows the quantum oscillations after subtraction of the linear background. (d): Sketch of the STO/SCO/LAO/STO structure.

2 μ A. Experiments were carried out in a dilution refrigerator and a pumped ^3He system with a rotatable sample stage.

Fig. 1(a)(i)–(c)(i) shows the longitudinal magnetoresistance ρ_{xx} of our samples at various temperatures, for magnetic fields aligned perpendicular to the xy plane. Clear oscillations with strongly temperature-dependent amplitudes are apparent in each case. The complex periodicities indicate that several frequencies are superposed. Fig. 1(a)(ii)–(c)(ii) show the same data as in (i), but with a smooth background removed. An example of the background subtracted for each sample is shown as a dashed line in the insets of these figures.

The Hall effect ρ_{xy} of each sample showed quantum oscillations similar to those in ρ_{xx} , on a large, approximately linear background. Fig. 1(c)(iii) shows data from S3. Apart from the oscillation amplitudes, ρ_{xy} is independent of temperature. By performing all measurements with both positive and negative magnetic field polarities, we exclude the possibility that the oscillatory Hall effect arises from an admixture of ρ_{xx} in ρ_{xy} , or vice versa. Observable quantum oscillations in the Hall effect are relatively unusual, but arise from the same Landau level-related phenomena as SdH oscillations in

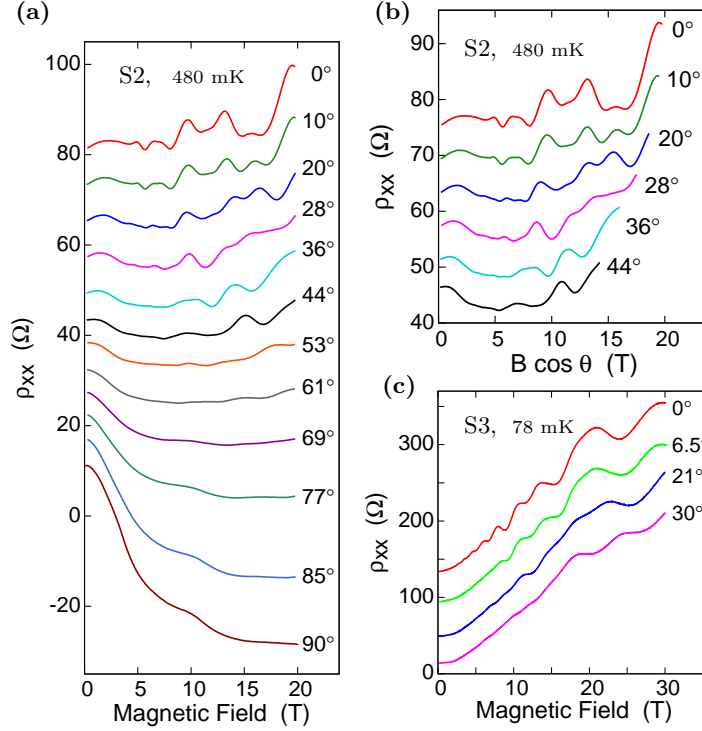


Figure 2. Dependence of SdH oscillations on magnetic field orientation. The angle θ between the magnetic field direction and the normal to the interface is shown beside each of the curves. (a) SdH oscillations at different tilt angles for sample S2, (b) SdH oscillations for sample S2 up to 44° (from (a)), as a function of the perpendicular field component $B \cos \theta$. (c) SdH oscillations at different tilt angles for sample S3. The curves are offset vertically for clarity.

ρ_{xx} [17]. Previous observations of this effect have been well documented, for example, in semi-metals [24] and, recently, as the first confirmed example of quantum oscillations in the high temperature cuprate superconductors [25].

Fig. 2 shows the dependence of ρ_{xx} on the angle θ between the magnetic field direction and the z -axis of the sample for S2 and S3 (data as a function of magnetic field orientation are not available for S1). The oscillations are rapidly suppressed, with a change in periodicity, as the magnetic field is tilted away from 0°. Over the wider range of angles measured for S2, we see the background magnetoresistance change from positive to negative, and observe the development of a pronounced feature in parallel field ($\theta = 90^\circ$) at ~ 11 T.

3. Data analysis and discussion

We first focus on analysis of the SdH oscillations in ρ_{xx} at $\theta = 0^\circ$, as shown in Fig. 1. These oscillations have amplitudes of the order of 10% of the total resistance, which suggests that Landau levels are not fully resolved in these systems, i.e. there is considerable overlap of levels. In this situation, SdH oscillations are sinusoidal in inverse

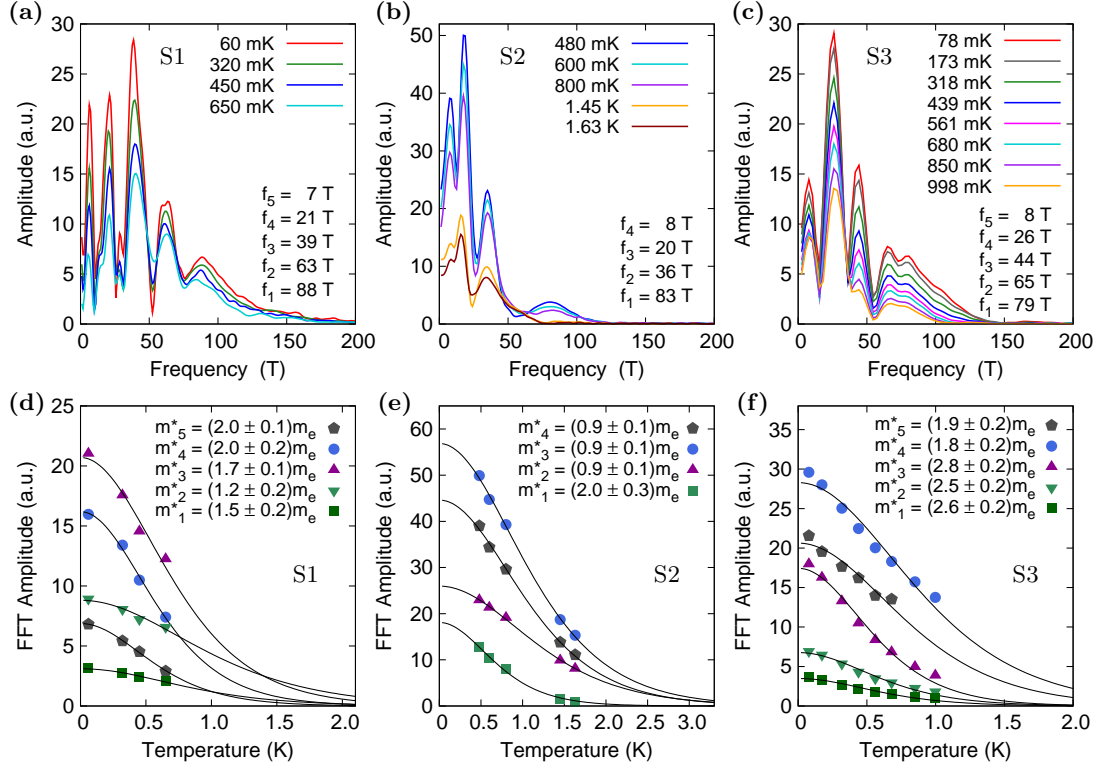


Figure 3. (a) Fourier transform between 4 and 30 T for sample S1. (b) Fourier transform between 4 and 20 T for S2. (c) Fourier transform between 4 and 30 T for S3. (d)–(f) Temperature dependence of the oscillation amplitudes with values of m^* in units of m_e . The solid lines are fits to $\alpha_i T / \sinh(\alpha_i T)$. Some of the data are rescaled so that all the data for each sample can be shown clearly on a single plot.

magnetic field $1/B$, and are described by the general expression [26, 17]

$$\Delta\rho_{xx} \propto \sum_i \exp(-\alpha_i T_{D_i}) \frac{\alpha_i T}{\sinh(\alpha_i T)} \sin\left(\frac{2\pi p f_i}{B} + \phi_i\right), \quad (1)$$

where T is temperature, and f and ϕ are the frequency and phase of the oscillations; p is the harmonic number. The amplitude factors contain the term $\alpha = 2\pi^2 p k_B m^* / \hbar e B$, and allow the effective mass m^* , and Dingle temperature T_D of the charge carriers to be extracted from the temperature and magnetic field dependence of the signal [17]. T_D is a measure of the quantum mobility μ , and can be expressed as $T_D = (e\hbar/2\pi k_B)(1/m^*\mu)$.

To analyse the ρ_{xx} data in Fig. 1, we subtracted a smoothly varying background from each of the curves to obtain $\Delta\rho_{xx}$, as shown, and performed Fourier transforms (FTs) in the inverse magnetic field. Fig. 3(a)–(c) gives the resulting Fourier spectra for the three samples, and shows that five peaks are visible in the FT for S1 and S3, and four for S2, corresponding to five or four distinct oscillation frequencies in the SdH signals.

The very low frequency oscillations, resolved as FT peaks at 7 T or 8 T, may be subject to some uncertainty due to the difficulty of achieving perfect background subtraction. However, in all three samples, the background has very weak or negligible

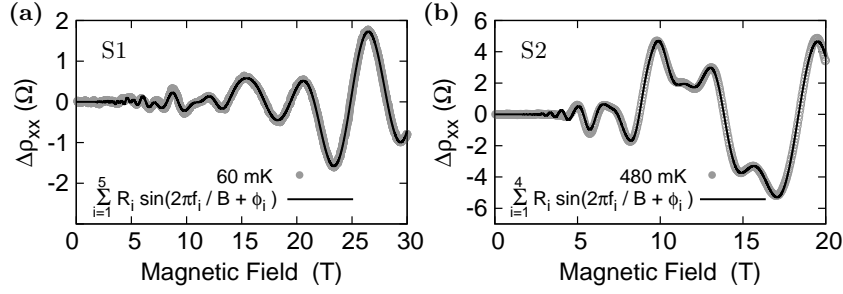


Figure 4. Fits of expression (1) to $\Delta\rho_{xx}$ for (a) S1 and (b) S2, using f_i and m_i^* from the Fourier transforms. The grey points show the measured data, and the solid lines represent the fits.

temperature dependence, compared to the strong temperature dependence of the amplitude of the 7 or 8 T peak, and none of the background curves we subtracted show any periodic component. We therefore treat the lowest frequency FT peak as a genuine component of the SdH signal in our samples. In the absence of harmonic content, which we will discuss below, the FT results indicate that five (S1, S3) or four (S2) high mobility conduction subbands contribute to the quantum transport in our samples. The observation of only four subbands for sample S2 may be a result of lower resolution in the FT due to the smaller magnetic field range of the measurement (0 - 20 T for S2, compared to 0 - 30 T for S1 and S3), or may be related to the slightly different structure of S2, which has one fewer LAO layers than S1 and S3.

By fitting the temperature dependence of the FT peak amplitudes to $\alpha_i T / \sinh(\alpha_i T)$, we extracted the carrier effective mass in each case (see Fig. 3(d)–(f)). FTs were taken over several magnetic field ranges for each sample, and the effective mass extracted for each range. The masses quoted in Fig. 3(d)–(f) are the mean values of m^* resulting from this procedure. In all cases, the experimental temperature dependence is well-described by the theoretical curves, and the errors given reflect the spread in the values of m^* over the full field range, rather than the quality of the fits.

If the SdH signal contains harmonics of a given oscillation, both the measured frequencies *and* the temperature dependence (we actually extract pm^* from the fits of $\alpha_i T / \sinh(\alpha_i T)$) should scale with the harmonic number p . This is not the case for any of the oscillations we observe in our samples, and we conclude that the peaks in the FTs correspond to fundamental frequencies, implying independent conduction channels. The frequencies and effective masses obtained from our analysis of the SdH oscillations are summarised in the first two columns of Table 1. We note that analysis of both the conductivity, calculated as $\sigma_{xx} = \rho_{xx} / (\rho_{xx}^2 + \rho_{xy}^2)$, and the oscillations in ρ_{xy} , gave the same results as analysis of ρ_{xx} for a given sample, within the experimental errors.

As a check of our Fourier analysis, we attempted to directly fit the oscillatory magnetoresistance with expression (1) using the frequencies and values of m_i^* extracted from the FTs. T_{D_i} , ϕ_i and an overall field-independent amplitude were used as fit parameters. The fits for S1 and S2 are shown in Fig. 4. Although the fits are not

Table 1. Subband properties derived from analysis of SdH oscillations in each of the three samples: SdH frequency f ; effective mass m^* ; carrier density n ; subband energy relative to the Fermi energy $E_F - E$; Dingle temperature T_D ; quantum mobility μ .
 * Subband f_5 of S1 reaches the quantum limit close to 10 T, which prevents us from extracting a reasonable measure of T_D and hence μ in this case.

Sample	m^* (m_e)	n (10^{12}cm^{-2})	$E_F - E$ (meV)	T_D (K)	μ (cm^2/Vs)
S1					
$f_1 = 88$ T	1.5(2)	4.3	6.9	3.55	401
$f_2 = 63$ T	1.2(2)	3.0	6.0	2.50	713
$f_3 = 39$ T	1.7(1)	1.9	2.7	0.40	3144
$f_4 = 21$ T	2.0(2)	1.0	1.2	0.38	2813
$f_5 = 7$ T	2.0(1)	0.3	0.4	-	-*
S2					
$f_1 = 83$ T	2.0(3)	4.0	4.8	1.86	558
$f_2 = 36$ T	0.9(1)	1.7	4.5	2.19	1085
$f_3 = 20$ T	0.9(1)	1.0	2.6	0.92	2609
$f_4 = 8$ T	0.9(1)	0.4	1.0	2.80	821
S3					
$f_1 = 79$ T	2.6(2)	3.8	3.5	-	-
$f_2 = 65$ T	2.5(2)	3.1	3.0	-	-
$f_3 = 44$ T	2.8(2)	2.1	2.9	-	-
$f_4 = 26$ T	1.8(2)	1.3	1.7	-	-
$f_5 = 8$ T	1.9(2)	0.4	0.5	-	-

perfect at very low field, they reproduce the data rather well, and suggest that the results of the FT are reliable. We can also use these fits of expression (1) to extract T_{Di} , and hence calculate approximate values of μ for each of the subbands in S1 and S2. These results are given in the final two columns of Table 1. We emphasise that the values of T_{Di} and μ_i are approximate, but they clearly show that the mobilities are different for different subbands. Moreover, the highest values of μ_i in each sample are in keeping with the magnetic field of ~ 5 T at which the quantum oscillations begin to appear. (This onset field depends broadly on the ratio of Landau level width to cyclotron energy, and is inversely proportional to the mobility of the carriers in the relevant subband.)

Although reasonable fits of expression (1) could be obtained for S1 and S2, it was not possible to achieve even a moderately good fit to $\Delta\rho_{xx}$ for S3, and we were therefore unable to extract values for T_{Di} and μ_i . SdH oscillations in S3 start to become resolvable just below 2 T, which indicates that the mobility of at least one subband in this sample must be considerably higher than in S1 or S2. In the limit of well-resolved Landau levels, with little or no overlap between neighbouring levels, SdH oscillations are still periodic in $1/B$ but are no longer sinusoidal, and the LK expression (1) ceases to be valid. It is therefore possible that the failure of (1) for S3 is related to the higher mobility of

carriers in this sample.

As a brief comment on the possible contribution of spin-splitting to the SdH signals in our LAO/STO samples, we note that for the usual, field-linear Zeeman splitting of the Fermi surface, quantum oscillations can only provide information about spin-splitting and the g -factor of a system in certain specific circumstances: when so-called ‘spin-zeroes’ are observed; when the *absolute* oscillation amplitudes are accurately known; or when the signals contain significant harmonic content [17]. None of these circumstances apply in our measurements, and we are not aware of any evidence of non-linear splitting of the Fermi surface in LAO/STO. We therefore conclude that spin-splitting does not contribute in a resolvable way to the SdH signals we observe, so that, even though the Zeeman effect may be relatively large, we cannot extract information about the g -factor in our samples.

We now consider the magnetotransport in tilted magnetic fields. Fig. 2(a) shows ρ_{xx} for sample S2 as the magnetic field orientation is rotated from perpendicular to parallel to the plane of the LAO/STO interface. The suppression of the SdH oscillations as θ is increased shows that the conduction electrons are confined to the interface plane, such that quantum oscillations are generated only by the perpendicular component of the applied field. In the case of a single occupied subband, Landau level separation, and hence the period of the SdH oscillations, would be expected to scale with $1/B \cos \theta$. When multiple 2D subbands are occupied, however, mixing of Landau quantisation with the confinement potential leads to anti-crossings of discrete levels from different subbands as the field is tilted [27]. Landau level energies therefore show a complicated magnetic field dependence, which progressively modifies the periodicity of SdH oscillations as a function of θ . The data in Fig. 2(a) show just this behaviour, which can be clearly seen as a function of the perpendicular field component in Fig. 2(b), and confirm both the two-dimensionality of the electron system and the contribution to transport of multiple occupied subbands. We do not have data in tilted magnetic fields for sample S1, but data for S3 (Fig. 2(c)) show the same 2D, multi-subband behaviour.

It can be further seen from Fig. 2(a) that, as θ is increased towards 90° , the magnetoresistance of sample S2 becomes strongly negative and develops a significant drop at ~ 11 T. Similar behaviour in multi-subband semiconductor 2DEGs is attributed to a decreasing contribution of inter-subband scattering to the total resistance, as the parallel field component B_{\parallel} shifts the size confinement energies and depopulates the higher subbands. The so-called *diamagnetic shift* is given by

$$\Delta E_n = \frac{e^2 B_{\parallel}^2}{2m_n^*} | \langle z_n^2 \rangle - \langle z_n \rangle^2 |, \quad (2)$$

where the final term is the square of the spread of the electron wavefunction in the confinement direction for the n^{th} subband [28]. When the highest occupied subband is shifted across the Fermi energy, it depopulates completely and becomes unavailable to scattering processes, leading to a plateau and subsequent drop in ρ_{xx} [29, 30].

In order to estimate the diamagnetic shifts expected in sample S2, we have used a very simple model of a uniform triangular confining potential at the interface. The

similar masses measured for the three highest subbands in S2 suggest that they are split from the same conduction band, and, based on their energy spacing, we calculate an approximate value of 2.6×10^{-5} V/Å for the electric field confining the charge carriers in these three highest subbands. (The details of this calculation are given in the Supplementary Information.) The consequent energy shift would cause the highest subband to empty completely at $B_{\parallel} \sim 17$ T, which is quite close to the drop in resistance we observe at $B_{\parallel} \sim 11$ T, and supports a description of the magnetoresistance in terms of reduction of inter-subband scattering and depopulation of the highest subband as B_{\parallel} is increased. This suggests a very close analogy between the behaviour of the LAO/STO 2DEG and that of multi-subband semiconductor 2DEGs. A significant implication of this observation is that reducing the number of occupied subbands by other techniques, for example, via electric field control of the carrier density, should also lead to reduced inter-subband scattering and thus to higher mobility samples.

For a 2-dimensional electron system with parabolic conduction bands and circular Fermi surface sections, the frequency f_i of quantum oscillations is proportional to the carrier density in a given subband $n_i = N_v N_s e f_i / h$, where N_v and N_s are valley and spin degeneracy, respectively. We use this relation, assuming a single valley and twofold spin degeneracy, to calculate the carrier density for each of the subbands we have measured. We also use the corresponding 2D density of states to calculate the energies of the subband edges relative to the Fermi energy, $E_F - E_i = n_i \pi \hbar^2 / m_i^*$. These values are given in columns 3 and 4 of Table 1.

The total carrier density contributing to the SdH effect is similar for all three samples: $n_{SdH} = \sum_i n_i \sim 1 \times 10^{13} \text{cm}^{-2}$. This is considerably higher than n_{SdH} measured previously in LAO/STO [18, 19], and is close to the saturation density generally observed in conducting samples believed to be free from extrinsic carriers [31]. We cannot, however, straightforwardly extract values for the total carrier densities from our Hall effect data for comparison, as the Hall coefficient is necessarily a combination of contributions from multiple subbands with different mobilities, and must also comprise the effects of inter-subband scattering [32]. Naive calculations of ρ_{xy} based only on n_i and μ_i extracted from our SdH results show poor agreement with the experimental Hall data (see Supplementary Information).

Fig. 5 shows the subband energies ($E_F - E$) versus density of states for each of our samples. The most striking aspect of these subband structures is the small energy scale involved. The lowest subband edge is only a few millielectronvolts below the Fermi energy in each sample, and the separation of the subbands is mostly ~ 1 meV or less. We emphasise the observation of this small energy scale, as bandstructure calculations predict energies of at least an order of magnitude larger, in the range of tens to hundreds of meV, for the occupied conduction subbands in LAO/STO [20, 21, 22]. The calculated bandstructures assume that a full electronic reconstruction takes place at the interface, with the transfer from LAO to STO of 0.5 electrons per 2-dimensional unit cell [6, 2]. The large discrepancy between our measurement and calculated subband energies raises questions about both the predicted evolution of the conduction bandstructure, and the

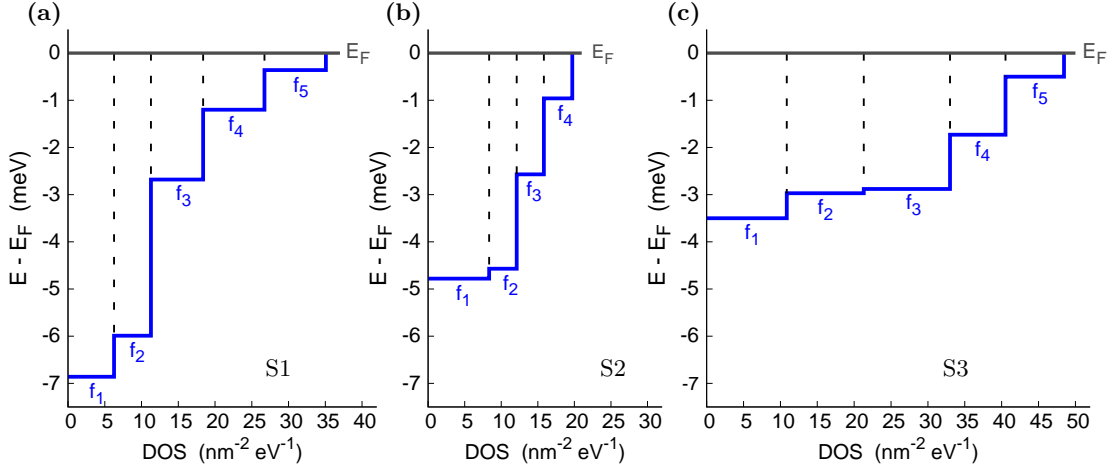


Figure 5. Density of states (DOS) for the multi-subband 2DEG in our three samples, extracted from analysis of the SdH oscillations. (a) Sample S1. (b) Sample S2. (c) Sample S3.

total carrier density possible in the 2DEG.

Although previous measurements on LAO/STO could clearly resolve only a single SdH frequency [18, 19], and so were unable to provide any information about the overall subband structure, SdH experiments on δ -doped STO [33, 34] reveal frequencies and effective masses in a similar range to those we observe in LAO/STO, and imply a similar energy scale for the subband structure. The subbands in electric-field-induced STO 2DEGs [35] were also found to be only a few meV below the Fermi energy for carrier densities close to $1 \times 10^{13} \text{ cm}^{-2}$. 2DEGs on the cleaved surface of STO, however, studied by angle-resolved photoemission (ARPES) experiments, have subband structures with band edges 100–200 meV below the Fermi energy and energy splitting of order tens to 100 meV [36, 37], perhaps suggesting a different character of the 2DEG in these surface systems. We note that the subband energies we observe in LAO/STO are at the limits of resolution for ARPES and related experiments, and may shed light on the failure, so far, to resolve the bandstructure at the LAO/STO interface using these techniques. The relatively weak confining potential implied by the small subband energies may also be reflected in the lower than expected core-level shifts observed in photoemission studies [13, 14, 15].

Fig. 5 and the results summarised in Table 1 show that there are small differences in both the bandstructure and the properties of the charge carriers between our three samples. We attribute this primarily to the differences in structure and growth conditions for each of the samples (see Supplementary Information), as varying the amount of LAO in the heterostructure, or the oxygen pressure during growth, has been shown to modify the properties of the 2DEG in several ways [38, 15, 12, 8, 9]. Of particular relevance to this work is that the number of LAO layers deposited and the density of defects such as oxygen vacancies affect the electric field which builds up across the polar LAO, and can thus be expected to directly affect the conduction band energies

at the interface [21, 20, 16].

The different effective masses we observe in a given sample are suggestive of subbands with different orbital character. The conduction bandstructure of bulk STO consists of three degenerate bands with minima at the gamma-point of the Brillouin zone, arising from the Ti 3d xy , xz and yz orbitals. The degeneracy of these bulk bands is lifted by a low temperature structural transition and by spin-orbit coupling [39], and further splitting into 2D subbands is expected with the introduction of the LAO interface and associated confinement potential. The d_{xy} -derived subbands are symmetric in the interface plane and give circular Fermi surfaces with light masses, whereas the $d_{xz/yz}$ subbands are expected to be weakly dispersing along one of the in-plane directions, and should lead to elliptical Fermi surfaces and heavy effective masses [20, 21, 22]. ARPES results on STO surface 2DEGs have yielded values of $\sim 0.7 m_e$ and $10\text{--}20 m_e$ for the light and heavy masses, respectively [36]. The masses we observe, however, are in a small range from $\sim 1\text{--}3 m_e$, and suggest that in LAO/STO we measure carriers in hybridised subbands, with mixed orbital character and masses intermediate between light and heavy. The differences between masses in different subbands should thus reflect the degree of hybridisation, and can be expected to depend sensitively on factors such as the detailed bandstructure and the spin-orbit coupling in a particular sample.

Even though we have measured three slightly different samples, the overall consistency of the picture we extract from our SdH results is notable. The number of subbands and the values of the SdH frequencies are very similar for the three samples, indicating similar Fermi surfaces as well as a comparable total carrier density in each case. The effective masses fall within a small range between ~ 1 and $3 m_e$, and, in all samples, the energy gaps between subbands are a few meV or less, with the lowest occupied subband less than ~ 7 meV below the Fermi energy. The general continuity of our results, despite the differences in sample structure and growth conditions, suggests that we are probing the intrinsic electronic behaviour of these LAO/STO 2DEGs. By revealing the detailed conduction bandstructure and the properties of the high mobility charge carriers, the results we have presented provide an opportunity to considerably advance our understanding of the formation and behaviour of this 2-dimensional electron system, and strongly motivate further related experimental and theoretical studies.

4. Summary

We have shown that multiple 2D subbands, with different effective masses and mobilities, are responsible for conduction in the LAO/STO 2DEG. We observed SdH oscillations consistent with those in previous work [18, 19], but have resolved and characterised several additional subbands and a correspondingly higher density of carriers contributing to quantum transport. This has allowed us to calculate the energies of successive subband edges, and reveals an energy scale more than an order of magnitude smaller than predicted by bandstructure calculations.

In tilted magnetic fields we find evidence of significant inter-subband scattering modified by a diamagnetic shift of the subband energies. This observation strengthens the analogy between LAO/STO and the behaviour of semiconductor 2DEGs, and suggests that reducing the number of occupied subbands may be a route to even higher mobility 2DEGs in this oxide system.

Acknowledgements

This work has been supported by the Stichting Fundamenteel Onderzoek der Materie (FOM) with financial support from the Nederlandse Organisatie voor Wetenschappelijk Onderzoek (NWO). AMC acknowledges support from a Marie Curie IIF grant.

References

- [1] Ohtomo A and Hwang H Y 2004 *Nature* **427** 423.
- [2] Mannhart J, Blank D H A, Hwang H Y, Millis A J, and Triscone J-M 2008 *MRS Bull.* **33** 1027.
- [3] Reyren N, Thiel S, Caviglia A D, Fitting Kourkoutis L, Hammerl G, Richter C, Schneider C W, Kopp T, Rüetschi A-S, Jaccard D, Gabay M, Triscone J-M, and Mannhart J 2007 *Science* **317** 1196.
- [4] Brinkman A, Huijben M, van Zalk M, Huijben J, Zeitler U, Maan J C, van der Wiel W J, Rijnders G, Blank D H A, and Hilgenkamp H 2007 *Nature Mater.* **6** 493.
- [5] Chen H, Kolpak A M, and Ismail-Beigi S 2010 *Adv. Mater.* **22** 2881.
- [6] Okamoto S and Millis A J 2004 *Nature* **428** 630.
- [7] Kalabukhov A, Gunnarsson R, Börjesson J, Olsson E, Claeson T, and Winkler D 2007 *Phys. Rev. B.* **75** 121404(R).
- [8] Siemons W, Koster G, Yamamoto H, Harrison W A, Lucovsky G, Geballe T H, Blank D H A, and Beasley M R 2007 *Phys. Rev. Lett.* **98** 196802.
- [9] Herranz G, Basletić M, Bibes M, Carrétéro C, Tafrá E, Jacquet E, Bouzehouane K, Deranlot C, Hamzić A, Broto J-M, Barthélémy A, and Fert A 2007 *Phys. Rev. Lett.* **98** 216803.
- [10] Willmott P R, Pauli S A, Herger R, Schlepütz C M, Martoccia D, Patterson B D, Delley B, Clarke R, Kumah D, Cionca C, and Yacoby Y 2007 *Phys. Rev. Lett.* **99** 155502.
- [11] Kalabukhov A, Boikov Yu A, Serenkov I T, Sakharov V I, Popok V N, Gunnarsson R, Börjesson J, Ljustina N, Olsson E, Winkler D, and Claeson T 2009 *Phys. Rev. Lett.* **103** 146101.
- [12] Huijben M, Brinkman A, Koster G, Rijnders G, Hilgenkamp H, and Blank D H A 2009 *Adv. Mater.* **21** 1665.
- [13] Yoshimatsu K, Yasuhara R., Kumigashira H, and Oshima M 2008 *Phys. Rev. Lett.* **101** 026802.
- [14] Segal Y, Ngai J H, Reiner J W, Walker F J, and Ahn C H 2009 *Phys. Rev. B* **80** 241107(R).
- [15] Takizawa M, Tsuda S, Susaki T, Hwang H Y, and Fujimori A 2011 *Phys. Rev. B* **84** 245124.
- [16] Singh-Bhalla G, Bell C, Ravichandran J, Siemons W, Hikita Y, Salahuddin S, Hebard A F, Hwang H Y, and Ramesh R 2011 *Nature Phys.* **7** 80.
- [17] Shoenberg D. *Magnetic Oscillations in Metals*. Cambridge University Press 1984.
- [18] Caviglia A D, Gariglio S, Cancellieri C, Sacépé B, Fête A, Reyren N, Gabay M, Morpugo A F, and Triscone J-M 2010 *Phys. Rev. Lett.* **105** 236802.
- [19] Ben Shalom M, Ron A, Palevski A, and Dagan Y 2010 *Phys. Rev. Lett.* **105** 206401.
- [20] Popović Z S, Satpathy S, and Martin R M 2008 *Phys. Rev. Lett.* **101** 256801.
- [21] Son W-j, Cho E, Lee B, Lee J, and Han S 2009 *Phys. Rev. B* **79** 245411.
- [22] Delugas P, Filippetti A, Fiorentini V, Bile D I, Fontaine D, and Ghosez P 2011 *Phys. Rev. Lett.* **106** 166807.

- [23] M Huijben, G Koster, H J A Molegraaf, M K Kruize, S Wenderich, J E Kleibeuker, A McCollam, V K Guduru, A Brinkman, H Hilgenkamp, U Zeitler, J C Maan, D H A Blank and G Rijnders, arXiv:1008.1896v1.
- [24] Reynolds J M, Hemstreet H W, Leinhardt T E, and Triantos D D 1954 *Phys. Rev.* **96** 1203.
- [25] Doiron-Leyraud N, Proust C, LeBoeuf D, Levallois J, Bonnemaïson J-B, Liang R, Bonn D A, Hardy W N, and Taillefer L 2007 *Nature* **447** 565.
- [26] Lifshitz I M and Kosevich A M 1956 *Sov. Phys. JETP* **2** 636.
- [27] J C Maan, in *Springer Series in Solid State Sciences 53*, edited by G Bauer, F Kuchar and H Heinrich (Springer Berlin, 1984) p. 183.
- [28] Beinvogl W, Kamgar A, and Koch J F 1976 *Phys. Rev. B* **14** 4274.
- [29] Englert Th, Maan J C, Tsui D C, and Gossard A C 1983 *Solid State Commun.* **45** 989.
- [30] Portal J C, Nicholas R J, Brummell M A, Cho A Y, Cheng K Y, and Pearsall T P 1982 *Solid State Commun.* **43** 907.
- [31] Thiel S, Hammerl G, Schmehl A, Schneider C W, and Mannhart J 2006 *Science* **313** 1942.
- [32] Zaremba E 1992 *Phys. Rev. B* **45** 14143.
- [33] Kozuka Y, Kim M, Bell C, Kim B G, Hikita Y, and Hwang H Y 2009 *Nature* **462** 487.
- [34] Kim M, Bell C, Kozuka Y, Kurita M, Hikita Y, and Hwang H Y 2011 *Phys. Rev. Lett.* **107** 106801.
- [35] Ueno K, Nakamura S, Shimotani H, Ohtomo A, Kimura N, Nojima T, Aoki H, Iwasa Y, and Kawasaki M 2008 *Nature Mater.* **7** 855.
- [36] Santander-Syro A F, Copie O, Kondo T, Fortuna F, Pailhès S, Weht R, Qiu X G, Bertran F, Nicolaou A, Taleb-Ibrahimi A, Fèvre P L Le, Herranz G, Bibes M, Reyren N, Apertet Y, Lecoeur P, Barthélémy A, and Rozenberg M J 2011 *Nature* **469** 189.
- [37] Meevasana W, King P D C, He R H, Mo S-K, Hashimoto M, Tamai A, Songsiriritthigul P, Baumberger F, and Shen Z-X 2011 *Nature Mater.* **10** 114.
- [38] Bell C, Harashima S, Hikita Y, and Hwang H Y 2009 *Appl. Phys. Lett.* **94** 222111.
- [39] Mattheiss L F 1972 *Phys. Rev. B* **6** 4740.

Supplementary Information

Sample growth

The SrTiO₃/SrCuO₂/LaAlO₃/SrTiO₃ heterostructures used in our study were grown by pulsed laser deposition, with the growth process monitored *in situ* by reflection high energy electron diffraction (RHEED). LaAlO₃ was deposited on a TiO₂-terminated single crystal SrTiO₃(001) substrate at 850 °C in an oxygen environment. Either the oxygen pressure during growth, or the number of LaAlO₃ layers was varied slightly between samples, as follows:

Sample	No. of LaAlO ₃ layers	O ₂ pressure during LaAlO ₃ growth
S1	10	2×10^{-3} mbar
S2	9	2×10^{-3} mbar
S3	10	1×10^{-5} mbar

The sample was cooled from 850 °C to 600 °C in the LaAlO₃ growth pressure at a rate of 50 °C/min, and a single monolayer of SrCuO₂ and two monolayers of SrTiO₃ were then deposited at 600 °C in 6×10^{-2} mbar of oxygen for all samples. This part of the growth procedure also acts as an annealing step for the LaAlO₃. The fluence of the laser pulses was 1.3 J/cm², the spot size was 1.76 mm² and the repetition rate was 1 Hz. The target-substrate distance was 50 mm. After growth, the samples were slowly cooled to room temperature in 6×10^{-2} mbar oxygen at a rate of 10 °C/min.

Hall effect

In figure 1 we show Hall effect data (solid lines) from all three samples. As described in the main paper, the Hall effect shows quantum oscillations, but is otherwise temperature independent and approximately linear in magnetic field - there is a slight change of slope between 3 T and 5 T in samples S1 and S2 .

Using the relaxation-time approximation to the Boltzmann transport equation, it is straightforward to derive the Hall effect expected in a multi-subband system [s1], which can be expressed in terms of the carrier densities and mobilities of each subband as follows:

$$\rho_{xy} = \left(\frac{1}{e} \right) \frac{\left(\frac{n_1 \mu_1^2}{1+(\mu_1 B)^2} + \frac{n_2 \mu_2^2}{1+(\mu_2 B)^2} + \dots \right)}{\left(\frac{n_1 \mu_1}{1+(\mu_1 B)^2} + \frac{n_2 \mu_2}{1+(\mu_2 B)^2} + \dots \right)^2 + B^2 \left(\frac{n_1 \mu_1^2}{1+(\mu_1 B)^2} + \frac{n_2 \mu_2^2}{1+(\mu_2 B)^2} + \dots \right)^2} B \quad (1)$$

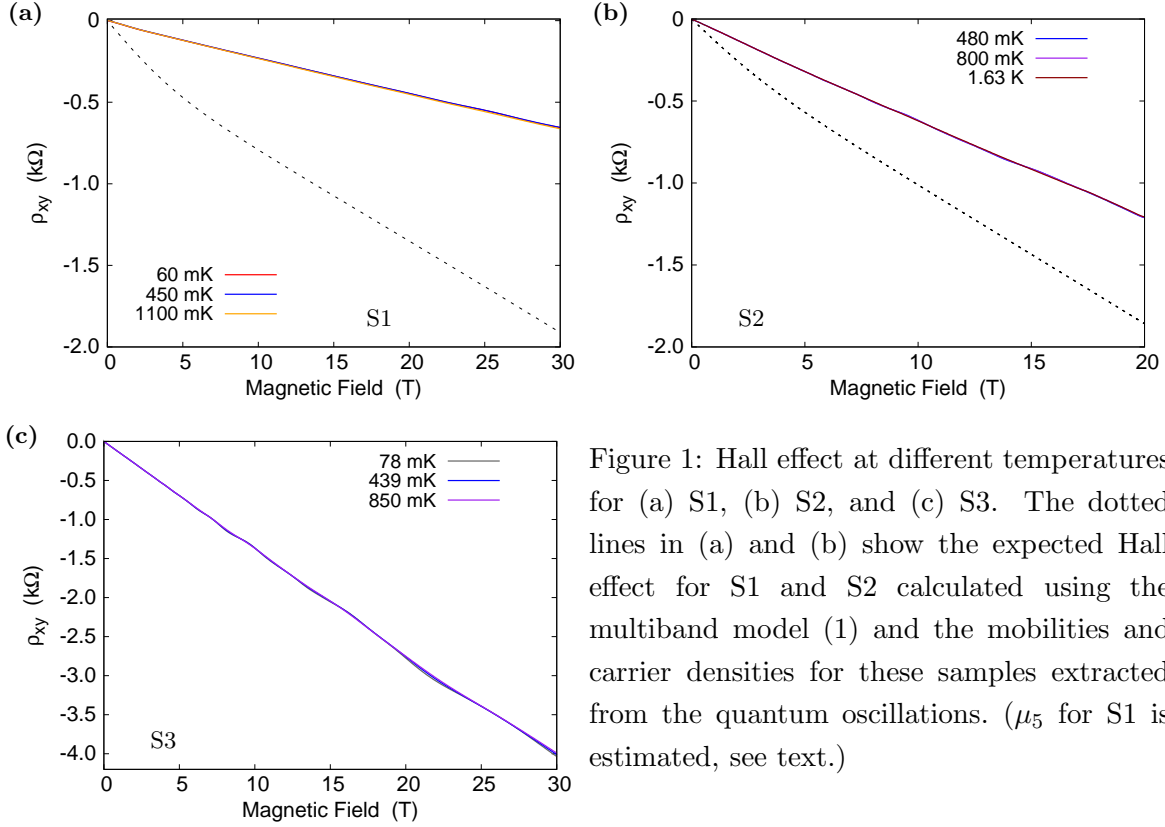


Figure 1: Hall effect at different temperatures for (a) S1, (b) S2, and (c) S3. The dotted lines in (a) and (b) show the expected Hall effect for S1 and S2 calculated using the multiband model (1) and the mobilities and carrier densities for these samples extracted from the quantum oscillations. (μ_5 for S1 is estimated, see text.)

The multiband Hall effect has, in general, a complicated dependence on the applied magnetic field, but reduces to a more familiar linear field dependence in the extreme low field/low mobility or high field/high mobility limits:

$$\rho_{xy} = \frac{n_1\mu_1^2 + n_2\mu_2^2 + \dots}{e(n_1\mu_1 + n_2\mu_2 + \dots)^2} B \quad (\mu_i B) \ll 1 \quad (2)$$

$$\rho_{xy} = \frac{1}{e(n_1 + n_2 + \dots)} B \quad (\mu_i B) \gg 1 \quad (3)$$

We note that $\mu_i B \equiv (\omega_c \tau)_i$, where $\omega_{c_i} = eB/m_i^*$ is the cyclotron frequency, and τ_i is the time between scattering events, or relaxation time, in a given subband.

The wide magnetic field range in our measurements means that the full expression (1) for ρ_{xy} should be the relevant one. In figures 1(a) and (b) we show, as dotted lines, ρ_{xy} calculated using this expression with μ_i and n_i extracted from the SdH data for S1 and S2 (main paper, Table 1). μ_5 for S1 is not available from our measurements, but is estimated as $1000 \text{ cm}^2/\text{V s}$. Due to the low carrier density in this subband, the value of μ_5 has a very weak influence on the shape of the curve.

For sample S3, we do not have values for μ_i but we can estimate the behaviour in the high field limit based on expression (3). This gives a high field Hall coefficient $R_H = 1/(en_{SdH}) = -58.3 \text{ m}^3/\text{C}$, where $n_{SdH} = \sum_i n_i$, and the n_i for S3 are given in

Table 1 of the main paper. The slope of the experimental Hall signal for S3, shown in figure 1(c), is considerably *steeper*, at $R_H = -136.4 \text{ m}^3/\text{C}$.

The discrepancies between the calculated and experimental curves suggest that effects such as inter-subband scattering [s2], or the presence of additional occupied subbands which do not contribute to the SdH effect, may need to be taken into account in any description of the Hall effect in this system.

It is clear from expression (1) that an oscillatory Hall coefficient can be expected in a system with multi-band transport, where one or more of the bands have an oscillatory conductivity (mobility). The oscillatory Hall effect therefore has the same origin as the SdH effect in ρ_{xx} . As can be seen from figure 1, the oscillations we observe in our samples are very small compared to the large non-oscillatory Hall signal (of order 1% or less), but their amplitudes are comparable to the amplitudes of the oscillations in ρ_{xx} for each sample.

Modeling the diamagnetic shift in B_{\parallel}

For sample S2 in tilted magnetic fields, we observe a strong negative magnetoresistance which develops a plateau and downward step for $B_{\parallel} \sim 11 \text{ T}$ (see Fig. 2 of the main paper). This behaviour typically indicates the reduction of inter-subband scattering and depopulation of the highest subband due to diamagnetic shift of the subband energies in a magnetic field parallel to the 2DEG [s3, s4, s5]. The diamagnetic shift expected for electrons in the n^{th} subband is given by

$$\Delta E_n = \frac{e^2 B_{\parallel}^2}{2m_n^*} | \langle z_n^2 \rangle - \langle z_n \rangle^2 |,$$

which is expression (2) in the main paper. $| \langle z_n^2 \rangle - \langle z_n \rangle^2 |$ is the square of the spread of the electron wavefunction in the z -direction.

In order to try and quantify this effect in our sample, we have constructed a very simple model of the confinement at the interface based on a band model of 2D electrons which are free in the xy -plane and confined in the z -direction, in analogy to the well-known situation in semiconductor heterostructures.

The three highest subbands in S2 have similar effective masses of $m^* \sim 0.9 m_e$ (Table 1, main paper), which suggests that they are split from the same bulk conduction band due to confinement at the interface. The energy spacing we have measured for these subbands implies a triangular confining potential $V(z) = eFz$, where F is the electric field at the interface.

The wavefunctions in a triangular potential are Airy functions and their solutions are well known to be

$$\zeta_n(z) = \text{Ai} \left(\frac{2m_z^* eF}{\hbar} \left(z - \frac{E_n}{eF} \right) \right)$$

[s6, s7], with eigenvalues

$$E_n \sim \left(\frac{\hbar^2}{2m_z^*} \right)^{1/3} \left(\frac{3\pi eF}{2} \left(n + \frac{3}{4} \right) \right)^{2/3} \quad n = 0, 1, 2, \dots$$

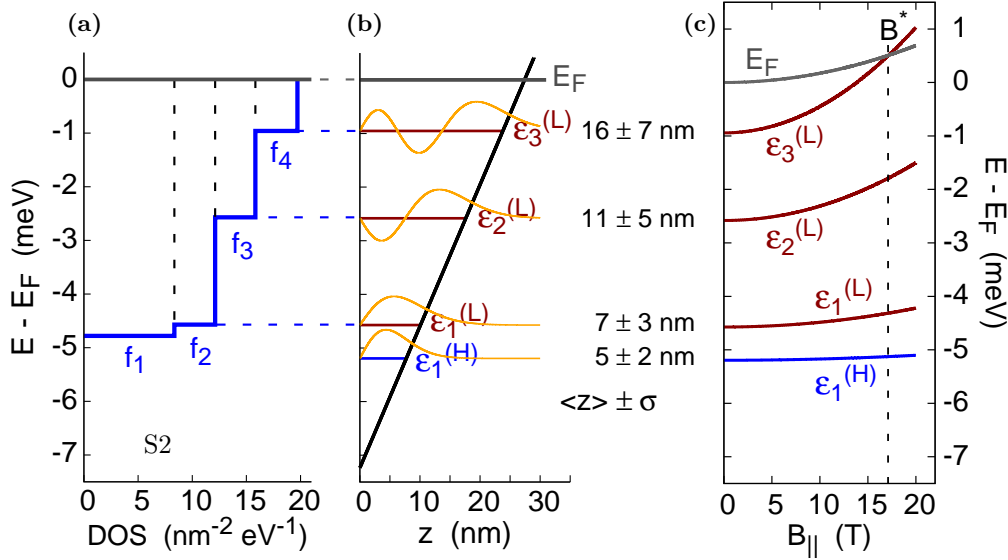


Figure 2: (a) Subband structure for the 2DEG in sample S2, derived from analysis of the SdH oscillations. (b) Potential well structure estimated from the subband spacing in S2. The wavefunction (in arbitrary units) and average z -position corresponding to each subband in this model are also shown; $\sigma = \sqrt{|\langle z_n^2 \rangle - \langle z_n \rangle^2|}$ is the spatial extent of the wavefunction. (c) Evolution of subband energies in the potential well of (b) due to the expected diamagnetic shift.

These wavefunctions and eigenvalues depend on m_z^* , rather than the in-plane effective mass m_{xy}^* that we extract from our SdH data. The lightest charge carriers in LAO/STO (and in bulk STO) are expected to occupy conduction bands with d_{xy} symmetry and $m_z^* > m_{xy}^*$. We do not have values of m_z^* for our samples, and therefore use a ratio of $m_z^*/m_{xy}^* \sim 2$, based on SdH results in bulk (Nb doped) STO [s8]. Although the lowest subband in S2 has a heavier effective mass of $2 m_e$, this is still relatively light, and we assume that this subband also has predominantly xy character. For convenience, we label the subbands (L) (for $m^* = 0.9m_e$) and (H) (for $m^* = 2m_e$). Using the energy spacing of the three (L) subbands (column 4 of Table 1 in the main paper), and assuming $n = 0, 1$ and 2 , we calculate a value of $F = 2.6 \times 10^{-5} \text{ V/\AA}$ for S2.

The potential well structure described by this model is shown in figure 2(b), including sketches of the wavefunction for each subband. We emphasise that this model is approximate, but comparison with figure 2(a), which shows the measured subband structure for S2 (taken from Fig. 5 in the main paper), shows that it reproduces the overall spacing of the subbands rather well. Taking the average values $\langle z_n \rangle = 2E_n/3eF$ and $\langle z_n^2 \rangle = 6/5 \langle z_n \rangle^2$ [s6, s7], we then calculate the diamagnetic shifts expected for each of the subbands, based on the potential well in figure 2(b). Figure 2(c) gives the resulting subband energies as a function of magnetic field parallel to the interface, and shows that the highest subband is expected to empty completely at $B^* \sim 17 \text{ T}$.

The value of $B^* \sim 17$ T is in quite good agreement with the drop in magnetoresistance we observe in sample S2 at $B_{\parallel} \sim 11$ T (Fig. 2(a), main paper), and supports an explanation of this feature as arising from depopulation of the highest subband.

In the triangular potential shown in figure 2(b), the $n = 1, 2$ subbands with $m^* = 2 m_e$ would also be expected. These are not observed, but lower mobilities for the slightly heavier carriers may explain their absence, as these carriers would then contribute only weakly, or not at all, to the SdH oscillations. The presence of these subbands would not significantly affect our estimate of B^* , only shifting it to slightly lower field.

The model potential well in figure 2(b) also provides an estimate of the thickness of the electron gas, and we show the average distance of carriers from the interface $\langle z \rangle$ with the spatial extent of each wavefunction at the right hand side of the figure. These values are consistent with the thicknesses of LAO/STO 2DEGs measured by other techniques [s9, s10], particularly when we consider that 80% of the carriers we observe are accommodated in the lowest two subbands.

Finally, we note that there is growing evidence of a large number of localised charge carriers in the LAO/STO 2DEG [s11, s12, s13], and that these carriers are expected to be more closely confined to the interface than the mobile carriers contributing to transport [s14, s15]. This would suggest a real confining potential which is non-uniform, and considerably steeper at the bottom of the well, with the localised carriers occupying lower-lying subbands than those we observe in the SdH effect. We do not consider this picture in detail, but such a scenario is not expected to significantly affect the conclusions we have drawn here about the high-mobility carriers we have measured in this LAO/STO system.

References

- [s1] N W Ashcroft and N D Mermin, *Solid State Physics* (Harcourt Brace College Publishers, 1976).
- [s2] E Zaremba, Phys. Rev. B **45**, 14143 (1992).
- [s3] W Beinvogl, A Kamgar and J F Koch, Phys. Rev. B **14**, 4274 (1976).
- [s4] J C Portal, R J Nicholas, M A Brummell, A Y Cho, K Y Cheng and T P Pearsall, Solid State Commun. **43**, 907 (1982).
- [s5] Th Englert, J C Maan, D C Tsui and A C Gossard, Solid State Commun. **45**, 989 (1983).
- [s6] F Stern, Phys. Rev. B **5**, 4891 (1972).
- [s7] T Ando, A B Fowler, and F Stern, Rev. Mod. Phys. **54**, 437 (1982).
- [s8] B Gregory, J Arthur, and G Seidel, Phys. Rev. B **14**, 4274 (1976).
- [s9] N Reyren, S Thiel, A D Caviglia, L Fitting Kourkoutis, G Hammerl, C Richter, C W Schneider, T Kopp, A-S Rüetschi, D Jaccard, M Gabay, J-M Triscone, and

- J Mannhart, *Science* **317**, 1196 (2007).
- [s10] M Basletic, J-L Maurice, C Carrétéro, G Herranz, O Copie, M Bibes, É Jacquet, K Bouzehouane, S Fusil, and A Barthélémy, *Nature Mater.* **7**, 621 (2008).
- [s11] A Brinkman, M Huijben, M van Zalk, J Huijben, U Zeitler, J C Maan, W G van der Wiel, G Rijnders, D H A Blank and H Hilgenkamp, *Nat. Mater.* **6**, 493 (2007).
- [s12] J A Bert, B Kalisky, C Bell, M Kim, Y Hikita, H Y Hwang and K A Moler, *Nat. Phys.* **7**, 767 (2011).
- [s13] M Takizawa, S Tsuda, T Susaki, H Y Hwang and A Fujimori, *Phys. Rev. B* **84**, 245124 (2011).
- [s14] Z S Popović, S Satpathy, and R M Martin, *Phys. Rev. Lett.* **101**, 256801 (2008).
- [s15] W-j Son, E Cho, B Lee, J Lee and S Han, *Phys. Rev. B* **79**, 245411 (2009).